DOI: 10.1002/cphc.200700169

Nanoscale Organization of the Pathogen Receptor DC-SIGN Mapped by Single-Molecule High-Resolution Fluorescence Microscopy

Bärbel I. de Bakker,[b] Frank de Lange,[c, d] Alessandra Cambi,[c] Jeroen P. Korterik,[b] Erik M. H. P. van Dijk,[b] Niek F. van Hulst,[e, f] Carl G. Figdor,[c] and Maria F. Garcia-Parajo*[a, f]

DC-SIGN, a C-type lectin exclusively expressed on dendritic cells (DCs), plays an important role in pathogen recognition by binding with high affinity to a large variety of microorganisms. Recent experimental evidence points to a direct relation between the function of DC-SIGN as a viral receptor and its spatial arrangement on the plasma membrane. We have investigated the nanoscale organization of fluorescently labeled DC-SIGN on intact isolated DCs by means of near-field scanning optical microscopy (NSOM) combined with single-molecule detection. Fluorescence spots of different intensity and size have been directly visualized by optical means with a spatial resolution of less than 100 nm. Intensity- and size-distribution histograms of the DC-SIGN fluorescent spots confirm that approximately 80% of the receptors are organized in nanosized domains randomly distributed on the cell membrane. Intensity–size correlation analysis revealed remarkable heterogeneity in the molecular packing density of the domains. Furthermore, we have mapped the intermolecular organization within a dense cluster by means of sequential NSOM imaging combined with discrete single-molecule photobleaching. In this way we have determined the spatial coordinates of 13 different individual dyes, with a localization accuracy of 6 nm. Our experimental observations are all consistent with an arrangement of DC-SIGN designed to maximize its chances of binding to a wide range of microorganisms. Our data also illustrate the potential of NSOM as an ultrasensitive, high-resolution technique to probe nanometer-scale organization of molecules on the cell membrane.

Introduction

Dendritic cells (DCs) play a central role in both innate and adaptive immune response. They are equipped with a variety of dynamically regulated pathogen-recognition receptors. While toll-like receptors have been recognized as ancient evolutionary pathogen receptors,[1] recent findings indicate that C-type lectins also play an important role in pathogen recognition and uptake.[2,3] The DC-specific intercellular adhesion molecule (ICAM) grabbing nonintegrin (DC-SIGN; CD209) is a recently identified C-type lectin involved in several types of DC interactions. DC-SIGN, exclusively expressed in DCs, is a type II transmembrane protein containing a mannose-binding domain that forms the ligand-binding site.[4,5] In the past few years, several studies highlighted the extraordinary pathogen-recognition capabilities of DC-SIGN. In addition to high-affinity binding to human immunodeficiency virus (HIV-1) envelope glycoprotein gp120,[6] DC-SIGN has been shown to mediate binding to several other viruses[7–11] and microorganisms.[12–17]

Although significant information on the structure of DC-SIGN is already available,[18,19] it remains largely obscure how this receptor is capable of efficiently recognizing such a large range of microorganisms. Recent in vitro biochemical experiments indicated that binding of DC-SIGN to hepatitis C virus glycoprotein E2 is enhanced by the formation of dimers and tetramers.[10,20] Using immuno electron microscopy (EM), we have recently shown that DC-SIGN organizes in well-defined microdomains on the cell surface of immature DCs (imDCs).[21] Furthermore, we showed that this type of arrangement is crucial for binding HIV-1 particles in situ.[21] These observations

[a] *Prof. M. F. Garcia-Parajo*
IBEC-Institut de Bioenginyeria de Catalunya & CIBER
Barcelona Science Park (PCB), Josep Samitier 1-5, 08028 Barcelona (Spain)
Fax: (+34) 93-4037181
E-mail: mgarcia@pcb.ub.es

[b] *Dr. B. I. de Bakker, J. P. Korterik, Dr. E. M. H. P. van Dijk*
Applied Optics Group, Faculty of Science & Technology
MESA+ Institute for Nanotechnology
University of Twente (The Netherlands)

[c] *Dr. F. de Lange, Dr. A. Cambi, Prof. C. G. Figdor*
Department of Tumor Immunology
Nijmegen Center for Molecular Life Sciences
University Medical Center, Nijmegen (The Netherlands)

[d] *Dr. F. de Lange*
Department of Radiology
Radboud University Nijmegen Medical Centre
Nijmegen (The Netherlands)

[e] *Prof. N. F. van Hulst*
ICFO-Institut de Ciències Fotòniques, 08860 Barcelona (Spain)

[f] *Prof. N. F. van Hulst, Prof. M. F. Garcia-Parajo*
ICREA-Institució Catalana de Recerca i Estudis Avançats
08010 Barcelona (Spain)

imply that the function of DC-SIGN as a viral receptor is greatly influenced by its nonrandom arrangement on the cell membrane, which prompted us to perform a detailed investigation of the spatial organization of DC-SIGN using an ultrasensitive fluorescence imaging technique capable of nanometer-scale resolution.

To date, fluorescence microscopy remains the most widely used technique to investigate the organization of receptor molecules at the cell surface; its applicability is enhanced by the use of autofluorescent proteins (XFP) in living cells.[22,23] Unfortunately, due to diffraction-limited resolution, confocal and epifluorescence microscopy are not suitable to probe the nanoscale organization of membrane components at physiologically relevant packing densities. Recent approaches in optical microscopy to break this diffraction limit include near-field microscopy,[24] stimulated emission depletion,[25] saturated structured illumination,[26] and single-molecule fluorescence photoactivation and photobleaching.[27] Each of these techniques has its specific advantages in terms of increased lateral and/or axial resolution but also has downsides with regard to technical complexity and/or limited application to a broad range of biological problems. Therefore, continuous efforts are focused on the improvement of existing methods and development of new techniques to bring the benefits of fluorescence microscopy to ultrahigh-resolution biological imaging.

Near-field scanning optical microscopy (NSOM) is a lensless optical imaging technique that provides simultaneous optical and topographic lateral resolution beyond the diffraction limit of light.[24,28–30] The technique is based on local excitation of the sample with a subwavelength light source that is raster-scanned over the surface. The lateral resolution is limited to the dimension of the aperture (typically ca. 70 nm), while the axial resolution is defined by the diffraction of the evanescent field emanating from the aperture (<50 nm), which results in an overall reduction of the illumination volume of more than 100-fold below the diffraction limit. As such, the technique is particularly suitable for investigating the distribution of membrane components on the cell surface in aqueous solutions with nanometer precision and single-molecule detection sensitivity.[28,30] Herein, we report on the application of NSOM combined with single-molecule detection (SMD) to investigate the spatial arrangement of receptor molecules on the membrane of intact DCs. We confirm the organization of DC-SIGN in clusters typically 180 nm in size. By means of SMD we have built up intensity distributions of all fluorescent spots and thus derived the relative number of proteins that are monomeric versus clustered in domains. Finally, we used single-molecule photobleaching in combination with a near-field-imaging, subtractive-fit method to investigate the intermolecular organization of DC-SIGN clusters. Our results are consistent with the notion that DC-SIGN clustering is necessary to enhance pathogen binding. Our experimental approach can be equally applied to many other membrane proteins and lipid domains and thus contribute to the understanding of the current model for the nanoscale organization of the cellular membrane.

Results and Discussion

High-Resolution Imaging of DC-SIGN

Typical fluorescence measurements on an imDC expressing DC-SIGN at the cell surface are shown in Figures 1B and C. The typical structure of the imDC, with numerous and extended fine dendrites, is clearly observed in the confocal image shown in Figure 1B. The high fluorescence intensity results from the high expression level of DC-SIGN and a considerable contribution from cell autofluorescence. The smallest visible features have a diffraction-limited size of about 350 nm. From the confocal image, it is hard to distinguish isolated components on the cell surface. By contrast, the high-resolution near-field image (Figure 1C) shows the distribution of DC-SIGN in greater detail. Figure 1C is a combined topograph (gray) and near-field image (color) of the frame highlighted in Figure 1B. The height of the dendrite regions varies from 10 nm to approximately 3 μm, as determined from the topographic image, and

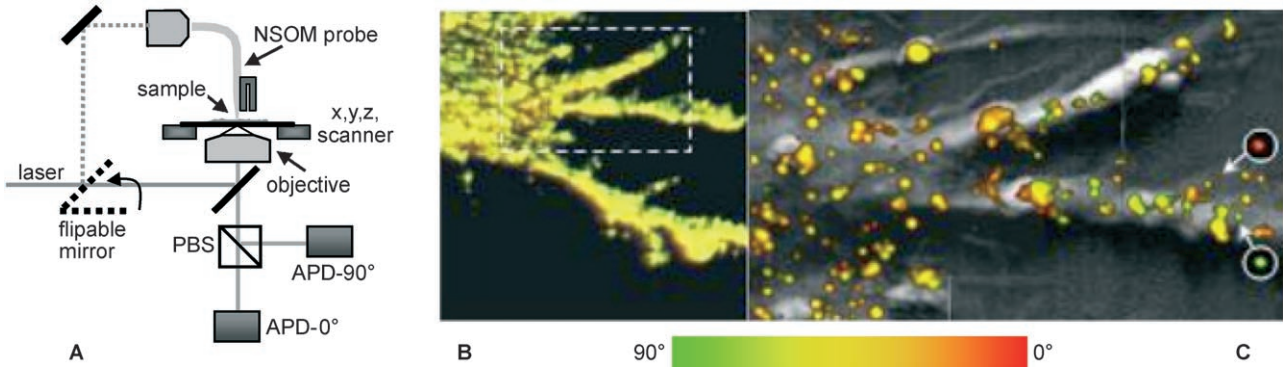

Figure 1. A) Schematic depiction of the single-molecule-sensitive confocal/NSOM setup (see the Experimental Section for details). B) Confocal image (20×20 μm^2) of a DC stretched on fibronectin-coated glass expressing DC-SIGN on the membrane. C) Combined topograph (gray) and near-field fluorescence image (color) of the frame highlighted in (B) (12×7 μm^2). In both (B) and (C), the fluorescence signal is color-coded according to the detected polarization (red for 0° and green for 90°). To illustrate the single-molecule detection sensitivity of the setup, we have slightly enlarged and rescaled the intensity of two individual molecules in the image [shown in circles in (C)]. Individual molecules are identified by their unique dipole emission (i.e. red and green color coding). The yellow color of most fluorescent spots results from additive emission of multiple molecules with random in-plane orientation (combination of red and green) in one spot.

this also shows that the cell is nicely stretched on the substrate without indications of filopodia/microvilli features. As observed in Figure 1C, fluorescence spots decorate the dendrite regions as well as the cell body in an apparently random fashion. The smallest near-field fluorescent spot is about 100 nm in size, comparable to the size of the probe aperture. In addition, the shallow penetration depth of the evanescent field guarantees exclusive excitation of the cell surface and thereby suppresses the large contribution of the cytoplasm fluorescence. Due to the small illumination volume of the probe, closely packed molecules are spatially resolved. As can be clearly seen in Figure 1C, the fluorescence spots differ in brightness, size, and emission polarization. These findings confirm and extend our previous observations that DC-SIGN is not randomly distributed as individual molecules but rather clustered in domains.[21] It also demonstrates that NSOM is equally capable (as compared to EM) to resolve the static heterogeneity of the cell membrane with high resolution. Moreover, as a surface-scanning technique, NSOM is able to follow the cell topology and thereby exclude any possible artifacts due to membrane structure or folding, in contrast to EM, which is exclusively a two-dimensional (2D) technique.

To show that clustering of DC-SIGN is not an artifact due to the drying procedure, we also studied the organization of DC-SIGN on imDCs and intermediate DCs by immuno-EM, using similar sample preparation to that described herein. While intermediate DCs showed a random distribution of DC-SIGN on the membrane, imDCs exhibited a clustered type of DC-SIGN organization.[21] These observations rule out sample preparation and/or drying as the source of DC-SIGN aggregation. This result is also consistent with NSOM experiments on fixed cells kept in fixative solution showing similar DC-SIGN clustering on imDCs.[30] Furthermore, experiments were performed with cells stretched on both fibronectin and poly-L-lysine substrates, and no substrate-dependent differences in the distribution of DC-SIGN were observed.

DC-SIGN is Organized in Nanometer-Sized Domains

To study the spatial organization of DC-SIGN in detail, we examined the fluorescence intensity and physical size of each individual spot using a semiautomated approach. The total photon count rate from a spot is directly related to the number of Cy5 dye molecules and thus to the number of DC-SIGN molecules. To analyze the fluorescence intensity, we integrate all photon counts within a contour of about 15% of the peak intensity of a given spot, subtract the background from a similar area in the vicinity of that spot, and finally divide by the total fluorescence acquisition time of the spot (see the Experimental Section for details). All spot intensities are collected in the histogram shown in Figure 2A. The spot intensities range from less than 5 kcounts s^{-1} to 1000 kcounts s^{-1}; this result indicates a large spread in the number of Cy5 dye molecules per spot. The low-intensity part of the total histogram is expanded in the inset of Figure 2A, which also includes the distribution of intensities that solely correspond to single-molecule spots (see the Experimental Section). The peak of the

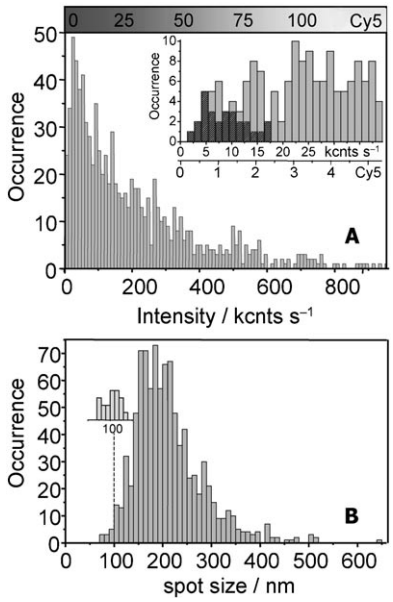

Figure 2. A) Intensity distribution of all measured spots at an excitation intensity of 150 W cm^{-2}. The inset shows an enlargement of the lowest intensity values of the distribution (< 40 kcounts s^{-1}), together with the intensity of single-molecule spots (shaded histogram). The lower axis of the enlarged distribution and upper graded bar of the main intensity distribution correspond to the number of Cy5 molecules. B) Size distribution of all measured spots. The inset shows the size of 19 single-molecule spots.

single-molecule intensity histogram (ca. 7 kcounts s^{-1}) was then used to normalize the total intensity distribution in terms of the number of Cy5 molecules. The overall intensity distribution peaks at about 3.5 Cy5 molecules with an average value of about 30 Cy5 molecules. Considering an antibody–DC-SIGN binding efficiency of 0.5–1 and antibody labeling efficiency of about 3 Cy5 molecules per secondary antibody, as determined from independent single-molecule antibody experiments (data not shown), these results indicate that the average number of DC-SIGN molecules in a cluster is about 5–10. Moreover, the overall intensity distribution demonstrates that as much as 80% of DC-SIGN is clustered on the membrane, and each cluster hosts from a few to several tens of DC-SIGN molecules. Clustering of DC-SIGN was observed in all analyzed images (20 independent NSOM measurements over seven representative cells), and similar variability in terms of cluster intensity was obtained. These results are also in agreement with previously obtained TEM data on imDCs.[21]

To obtain further proof of the organization of DC-SIGN in clusters, we measured the size (full width at half maximum, FWHM) of all fluorescent spots. The resulting size distribution is shown in Figure 2B. A separate histogram containing only the FWHM of single-molecule spots is also shown (inset). The single-molecule histogram peaks at about 100 nm, consistent with the probe aperture size and clearly separate from the peak of the main size distribution. Since in NSOM the measured sizes result from a convolution between the probe aperture and the real size of the clusters, a deconvolution algorithm was applied by assuming, for simplicity, a Gaussian probe response centered at 100 nm. After deconvolution with

the probe aperture size, the spot sizes range from less than 10 up to 500 nm, with a mean value of about 185 nm. Taken together, both intensity and size analysis confirm that DC-SIGN is confined in nanometer-sized domains.

We note that the cluster sizes determined here are similar to those obtained by TEM[21] but slightly larger than those obtained by NSOM in aqueous solutions.[30] We believe that the small differences may be due to sample preparation (dry versus liquid). We cannot rule out that some individual DC-SIGN molecules in the vicinity of a cluster might be brought even closer (beyond our NSOM resolution) on cell drying and thus result in a larger measured size. On the other hand, the intensities obtained under both dry and liquid conditions are similar to each other, with an average of 30 and 25 fluorescent dye molecules per domain, respectively, which validates our main conclusion of DC-SIGN clustering on imDCs.

In vitro biochemical studies showed that DC-SIGN forms multimers.[20] These oligomers contain fewer molecules than the average number of DC-SIGN molecules per spot that we observed in our experiments. Although oligomerization of DC-SIGN at the cell surface might occur, it seems improbable that the observed clusters are exclusively due to oligomerization. In fact, the physical size and intensity of the clusters are more consistent with a higher level of organization in which recruitment of proteins to specific areas of the cell membrane increases the local concentration of DC-SIGN. As was recently shown, an increase in the local concentration of DC-SIGN likely serves to facilitate cell–pathogen binding, as intermediate DCs with a random distribution of individual DC-SIGN molecules on their surface showed impaired binding to viruslike particles and reduced HIV transmission to peripheral blood mononuclear cells.[21]

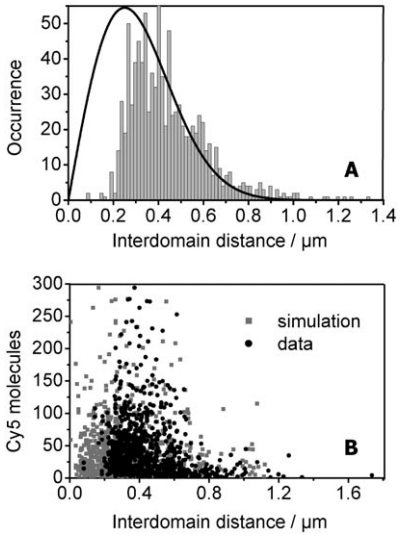

Figure 3. A) Interdomain distance distribution obtained by NND analysis of all measured fluorescence spots. The black solid line indicates a Poisson (random) distribution for a domain density of 2.53 domains μm^{-2}. B) Correlation between domain intensity (given as number of Cy5 molecules) and interdomain separation for measured and simulated data.

DC-SIGN Domains are Distributed Randomly on the Membrane

To investigate the distribution pattern of the domains on the cell surface, nearest neighbor distribution (NND) analysis was performed (see the Experimental Section). The area covered by domains represents about 8% of the total cell surface, which results in an average density of about 2.53 domains μm^{-2}. The NND between domains was measured and included in the distribution shown in Figure 3A. The distribution peaks at about 400 nm with a tail that extends up to 1.4 μm. The measurements were compared to a calculated NND of randomly distributed spots (Poisson) using the experimental domain density (solid line in Figure 3A). The overall shapes of the two distributions are similar, especially the tail of the distribution. The differences in shape between the experimentally obtained distribution and the simulated fitting for short intercluster distances are caused by the finite size of the domains, which impose a minimum on the experimentally measurable intercluster distances (ca. 200 nm, as shown in Figure 2B). The similar shapes of the two distributions strongly suggest a random distribution.

To conclusively rule out a possible nonrandom spatial distribution of the domains, we correlated the number of Cy5 molecules within a domain with the mutual domain separation (see Figure 3B). An apparent correlation emerges from the shape of the correlation plot, that is, large intensity values correlate with shorter interdomain distances and vice versa. To test the validity of this observation, we performed simulations by assigning random (*x,y*) coordinates to the experimentally measured domains and determining their intercluster separations. The overall simulated correlation plot is superimposed in Figure 3B. The similar shapes of the two correlation plots confirm our notion that DC-SIGN domains are randomly distributed on the membrane. The large wings in both intensity and interdomain distance in fact result from the large number of occurrences at about 400 nm and approximately 3.5 Cy5 molecules, respectively.

Heterogeneity in the Molecular Packing Density of DC-SIGN Domains

To study the molecular packing density of DC-SIGN in each domain, we performed correlation analysis between all fluorescent spot sizes and their respective intensities. The correlation plot is shown in Figure 4A. The vertical axis corresponds to the corrected size of each individual domain after deconvolution of the spot size with the NSOM probe response, and the horizontal axis corresponds to the number of Cy5 molecules per domain, as derived from Figure 2A. The presence of on average about 30 Cy5 molecules together with the average spot size of about 185 nm corresponds to a Cy5 density ρ of about 1000 Cy5 molecules μm^{-2}. The solid line in Figure 4A is plotted along all spots exhibiting this average density. A one-to-one relationship between size and intensity would indicate a constant molecular packing density within the domains, as expected for proteins existing in higher order oligomeric states and

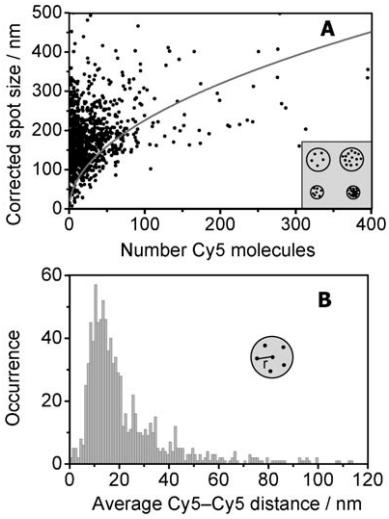

Figure 4. A) Correlation between the corrected spot size and intensity in terms of number of Cy5 molecules. Each point in the graph corresponds to one measured spot. The gray line shows the average molecular packing density. The sketch (inset) illustrates four types of domain packing: top left has a low packing density, while bottom right has a high packing density. The remaining two domains have similar packing density but are different in size and intensity. B) Intermolecular distance distribution r within domains under the assumption of random Cy5 ordering. The average intermolecular distance is about 22 nm.

observed for other transmembrane receptors investigated with the same technique (unpublished data). However, the molecular packing density of the DC-SIGN domains is remarkably heterogeneous, with physically large clusters containing only tens of Cy5 molecules, that is, low packing density (above the solid line in Figure 4A), and physically small clusters containing hundreds of Cy5 molecules, that is, high packing density (below the solid line).

To enquire into the molecular proximity of DC-SIGN within the domains, we calculated the average intermolecular distance r between Cy5 molecules in each domain using the relation $r \sim 1/(2\rho^{1/2})$ under the assumption of random distribution. The histogram in Figure 4B shows the average Cy5 intermolecular distance for all measured domains. The peak and average values of the distribution correspond to 12 and 22 nm, respectively. Clearly there is a maximum packing density of the Cy5 dye molecules dictated by their own size, the attached antibodies (ca. 10 nm), and the physical size of the DC-SIGN proteins. Although the use of antibody labeling precludes exact determination of the DC-SIGN intermolecular distances, it serves to accurately map the spatial organization of DC-SIGN and infer the distribution of DC-SIGN in the cluster. In fact, the shape of the distribution shown in Figure 4A also reflects organization of the antibody, and thus of DC-SIGN, in clusters, while the peak of the distribution agrees well with the physical size of the antibody. On the other hand, quantitative determination of antibody distances is difficult, since variations in Cy5 antibody labeling efficiency might occur. Similarly, owing to their physical size, the antibodies might spatially hinder each other if the proteins are too densely packed. Both effects could result in an under- or overestimation of the number of proteins involved in each cluster. Similar uncertainty is also obtained with EM. The use of autofluorescent proteins directly tagged to DC-SIGN in combination with NSOM should allow truly quantitative analysis of the stoichiometry of the clusters. Unfortunately, to date XFP labeling of DCs as nondividing primary cells remains a challenge.

Note that although NSOM provides greater resolution, the physical size of the domains is ultimately limited by the convolution with the NSOM probe size. Thus, the possibility always exists that small clusters, or even monomers, located at distances shorter than about 100 nm would be observed as larger clusters, which would shift the observed size distribution to higher values than is actually the case. Nevertheless, we believe from our data that the probability of the occurrence of smaller clusters at a higher packing density is rather low, since the fitting of the NND distribution to a Poisson (random) distribution has a peak value at about 300 nm. In any case, the existence of smaller clusters will not alter the main observation drawn from Figure 4, since the packing heterogeneity is mainly due to the large variation in the number of DC-SIGN units in each cluster and to a lesser extent caused by variations in the physical size of the clusters and their mutual proximity.

While the size of the domains is centered around 185 nm, the significant variation in the number of molecules in each domain, well beyond a purely random distribution (Poisson), reflects a large spread in Cy5 and thus in DC-SIGN in each cluster. Remarkably, the DC-SIGN domains are similar in size to most viruses (40–500 nm). If one relates the well-known capability of DC-SIGN to effectively bind to pathogens[6–17] and the already demonstrated importance of DC-SIGN clustering for virus binding,[21] our data strongly suggest a direct relationship between cluster size and the capacity of DC-SIGN for virus binding. That is, the large spread in DC-SIGN density per cluster may serve to maximize the chances of the DC binding to a large variety of viruses having different binding affinities. Along these lines, we have performed simulations to predict the capacity of pathogens of different sizes to establish interactions with either individual or clustered proteins. Interestingly, we found that particles with diameters in the range of most viruses known to bind to DC-SIGN (40–200 nm) bind with higher probability to clusters than to randomly distributed DC-SIGN. Furthermore, simulations of different cluster densities support the hypothesis that heterogeneity is beneficial for maximizing the chances of DC-SIGN binding to different pathogens (unpublished data).

Mapping the Intermolecular Organization of a Cluster

To directly assess the intermolecular organization of DC-SIGN, we performed sequential near-field fluorescence imaging in combination with single-molecule photobleaching. Recently, single-molecule confocal imaging has been applied to localize two identical dye molecules separated by 10–20 nm and immobilized on a background-free surface.[31] Since NSOM provides greater resolution and background suppression than confocal microscopy, we reckoned that a larger number of identical molecules could be spatially mapped with similar ac-

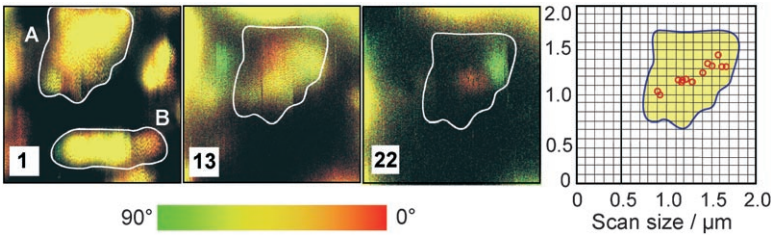

Figure 5. Selected near-field images over the same area taken at different moments in time (frames 1, 13, and 22); two exemplary domains (A and B) are highlighted. Scan area is 2×2 μm (256×256 pixels) at 5 ms per pixel acquisition time and 0.5 kW cm^{-2} excitation intensity. As an example, frame 22 shows two single-molecule fluorescence spots for which the center of mass has been determined with a precision of 6 nm. The rightmost grid shows the partial spatial reconstruction of domain A.

curacy on the membrane of intact cells. As a proof of principle, Figure 5 shows three representative near-field images of a DC-SIGN cluster obtained at different moments in time. Two DC-SIGN clusters are clearly observed in frame 1. While performing sequential imaging over the same area, photobleaching of Cy5 occurs and reduces the total fluorescence of the domain. Hence, frame 13 shows a discrete number of single-molecule fluorescent spots until finally only two Cy5 molecules are present in frame 22. To retrieve the spatial coordinates of individual molecules within a cluster, the following procedure was used. The (*x,y*) positions of single-molecule spots in the last frame (F_n) were determined by a 2D Gaussian fitting. The accuracy of localization of the single-molecule spots is 6 nm, limited by the signal-to-background ratio under our excitation conditions (ca. 500 W cm^{-2}). The pixel-by-pixel intensity of frame F_{n-1} was then subtracted from that of frame F_n. In doing so, we took special care to use the simultaneously obtained and corresponding topographic images to correct for any drift during the measurements. From the resultant subtracted near-field optical images, the (*x,y*) positions of new individual molecules were retrieved. The procedure was repeated as long as individual molecules and their coordinates could be discriminated from the subtracted near-field images. Following this procedure, the (*x,y*) positions of 13 distinct single-molecule spots within a region of approximately 1 μm^2 could be recovered (Figure 5, rightmost frame).

Distance analysis between adjacent Cy5 dye molecules in the cluster afforded a value of about 40±6 nm, which is within the range of the estimated intermolecular distances shown in Figure 4B, although it is an overestimation of the actual distance due to initial prebleaching. As observed from the reconstructed image, it appears that the Cy5 signal is distributed in small bunches rather than randomly. This type of organization most probably reflects the antibody distribution within the cluster. Further experiments using this approach in combination with XFP labeling should reveal the exact intermolecular organization of DC-SIGN.

Due to the diffraction-limited resolution of far-field microscopy, single-molecule experiments on cell membranes can be performed only after reducing the concentration of the fluorescently labeled proteins to typically less than 1 molecule μm^{-2}.[32] In our case, the increased resolution of NSOM enabled discrimination of individual molecules at much higher density (cluster in Figure 5), a convincing demonstration that the technique is ideally suited for the study of supramolecular complexes and/or protein oligomerization at physiologically relevant packing densities.

In essence, our experiments show the static heterogeneity of clustering by providing snapshots that map at a given moment the entire process of formation and degradation of domains and provide information on all possible situations. On the other hand, clustering should be a rather dynamic process, that is, clusters may change in size and density. If domain formation is a diffusion-assisted process, we should have observed in our static images some evidence of it, that is, the presence of "lower" intensity domains closer to "higher" intensity domains. However, we were not able to find such a correlation. As the organization of the DC-SIGN domains is random with no clear evidence for diffusion-assisted cluster growth, our data suggest that the DC-SIGN clusters may be targeted to the cell membrane in a preassembled way. One possible mechanism for this would be that intact DC-SIGN–raft clusters are delivered to the surface of imDC by means of transport vesicles from the trans-Golgi network.[33] Along these lines, biochemical data, copatching experiments, and ligand-binding essays in the presence or absence of methyl-β-cyclodextrin have indicated that about 50% of the total DC-SIGN population is raft-associated.[21] Dynamic high-resolution experiments performed with NSOM on living cell membranes should reveal whether preassembly or diffusion-assisted growth of DC-SIGN clusters takes place on imDCs. Along these lines, we recently showed that NSOM can operate in liquid environments without compromising resolution or sensitivity.[30] Currently we are extending the use of the technique to live imaging of XFP-labeled cells.

Conclusions

We have focused on the nanoscale organization of DC-SIGN on the membrane of immature DCs using high-resolution fluorescence microscopy combined with single-molecule detection sensitivity. Our experiments demonstrate the unique advantage of NSOM relative to confocal and electron microscopy when applied to densely packed systems on intact cells. The small illumination volume of NSOM allowed discrimination of isolated fluorescent spots of Cy5-labeled DC-SIGN on the surface of imDCs. By taking advantage of the single-molecule detection sensitivity of the setup, photon-count histograms of all fluorescent spots were built and related to the total number of fluorescent molecules contained in a given domain. Finally, by combining sequential NSOM imaging with discrete single-molecule photobleaching we were able to look inside an otherwise nonresolvable cluster and gain information on its intermolecular organization.

We have confirmed that more than 80% of the DC-SIGN proteins are organized in nanometer-sized domains. While the domain size matches the sizes of most viruses, the large heterogeneity in the molecular packing density of the domains may serve to maximize the chances of DC binding to a large variety of viruses having different binding affinities to DC-SIGN. It remains to be investigated how DC-SIGN is recruited to these regions and how the cell regulates the organization of DC-SIGN. Along these lines, we have performed experiments using the actin-disrupting agent cytochalasin D as well as the cholesterol-extracting agent methyl-β-cyclodextrin to test the influence of the cortical actin cytoskeleton and of lipid-raft integrity, respectively, but did not observe changes in DC-SIGN clustering on immature DCs.[21] Since there is increasing evidence that several pathogens exploit lipid platforms as docking sites to enter host cells,[34] we are currently employing high-resolution NSOM under liquid conditions to shed light on the raft hypothesis and provide quantitative information on the static and possibly dynamic compartmentalization of the cell membrane.

Experimental Section

Sample Preparation: imDCs were cultured from healthy human blood monocytes in the presence of IL-4 and GM-CSF, 500 and 800 U mL^{-1}, respectively (Schering-Plough, Brussels, Belgium). After 6 d of culture, flow-cytometry analysis showed low levels of CD14 and CD83, moderate levels of CD86, and high levels of MHC class I and II, consistent with the phenotype of imDCs. Obtained DCs were stretched on a fibronectin-coated glass cover slip for 1 h at 37 °C and fixed with 1% paraformaldehyde in phosphate-buffered saline (PBS) for 20 min. The specimens were rinsed in two washing steps with PBS and PBA (PBS containing 0.5% bovine serum albumin and 0.01% sodium azide). The cells were then incubated with homemade primary monoclonal antibodies (mAbs) AZN-D1 in PBA (10 mg mL^{-1}, 25 min). After two washing steps with PBA, a second incubation was performed with goat anti-mouse Cy5 (Jackson Immuno Research), 1:125 in PBA for 25 min, to allow fluorescence detection of the anti-DC-SIGN antibody. Antibody labeling efficiency as given by the manufacturer is 2–4 Cy5 molecules per antibody. Samples were subsequently post-fixed in 2% paraformaldehyde, dehydrated by subsequent incubations in 30, 50, 70, and 100% pure ethanol and finally critical-point dried.

High-Resolution, Single-Molecule Imaging of DC-SIGN: Cells were imaged with a combined confocal/near-field optical microscope with single-molecule detection sensitivity, as schematically shown in Figure 1A. Cy5-labeled DC-SIGN were excited either confocally or in near-field mode by using the 647 nm line of an Ar^+/Kr^+ ion laser (CW, Spectra-Physics). In confocal mode, incoming circularly polarized light is reflected by a dichroic mirror (650 DRLP Omega Optical Inc., Brattleboro VT) and focused onto the sample by an oil-immersion objective (Olympus, 64×, 1.4 N.A.) with a typical intensity of 150 W cm^{-2}. In the NSOM mode the excitation light is coupled into an Al-coated tapered fiber probe (single mode, $\lambda =$ 633 nm, Cunz, Frankfurt). The probe is kept within 10 nm of the sample by means of shear-force feedback providing simultaneously a topographic map of the sample surface.[28,30] A flippable mirror mount (Newfocus Inc.) enables switching between the two excitation modes. On the detection side, the collected light is appropriately filtered (665AELP, Omega Optical Inc., Brattleboro VT) and the fluorescence separated into two orthogonal polarization components (denoted the 0 and 90° components) by a broadband beam splitter (400–700 nm, Newport, Fountain Valley CA). Finally, the signal is focused onto two avalanche photodiodes (APDs, SPCM-100, EG&G, Quebec).

Individual cells were selected by bright-field illumination and subsequently imaged in confocal mode. Selected regions were then investigated by NSOM, with typical scanning speeds of 3–6 μm s^{-1}, depending on the surface roughness. The cell height in the dendrite region varied from tens of nanometers to a few micrometers, as derived from the shear-force signal. All data were acquired with the same near-field probe with an aperture size of about 100 nm, as determined from EM images. Presented data are based on seven representative cells and 20 different near-field scans.

Image Analysis: Near-field images were analyzed in a semiautomated fashion using custom-written software based on Labview (National Instruments, TX). In total, 1200 fluorescent spots were investigated in terms of their intensity, physical size, absolute position on the plasma membrane, and relative position with respect to each other. All spots were selected manually from the raw NSOM images. The intensity of each spot I_T (kcounts s^{-1}) was determined as $I_T = (I_s - I_b)/t$, where I_s is the sum of all photon counts within a contour of about 15% of the peak intensity level of a given spot, I_b the cell background from a similar area in the immediate vicinity of the spot, and t the total acquisition time of the fluorescent spot. The intensities were then related to the photon count rate detected from single Cy5 molecules, as inferred from spots exhibiting clear single-molecule signatures such as discrete bleaching, blinking, and unique dipole emission. Note that this method of obtaining the average intensity per spot assumes a random organization of DC-SIGN within the cluster. The size of each individual spot was determined by fitting the measured intensity profile with a 2D Gaussian function. The spot size was defined as the full width at half maximum (FWHM) of the fit. This approach works well as long as the spots are rather rounded and will be less accurate for irregularly shaped domains. However, from our NSOM images this is a good approximation, since the large patches are much less frequent and fall out of the main size distribution shown in Figure 2B. The positions of all spots on the cell membrane were determined by combining the near-field optical and topographic images, thereby allowing us to include in our data analysis only membrane-associated proteins. The simultaneously obtained topographic images were also used to exclude potential artifacts due to the structure of the cell membrane, such as steep cell edges or membrane folding. Mutual spot distances were examined by means of nearest-neighbor distance (NND) analysis, where the (x,y) position of each spot was determined from the peak position of a Gaussian fit to the intensity profile.

Acknowledgements

We are grateful to M. Koopman and F. van Leeuwen for fruitful discussions. B.I.dB. has been financed by the Netherlands Technology Foundation (STW). F.dL. and E.M.H.P.vD were supported by the Netherlands Foundation for Fundamental Research of Matter (FOM). A.C. was supported by the Netherlands Organization of Scientific Research, Earth and Life Sciences (SLW).

Keywords: high-resolution optical microscopy · lectins · membranes · receptors · single-molecule studies

[1] S. Akira, *Curr. Opin. Immunol.* **2003**, *15*, 5 – 11.
[2] P. D. Stahl, R. A. Ezekowitz, *Curr. Opin. Immunol.* **1998**, *10*, 50 – 55.
[3] K. Mahnke, M. Guo, S. Lee, H. Sepulveda, S. L. Swain, M. Nussenzweig, R. M. Steinman, *J. Cell Biol.* **2000**, *151*, 673 – 684.
[4] B. M. Curtis, S. Scharnowski, A. J. Watson, *Proc. Natl. Acad. Sci. USA* **1992**, *89*, 8356 – 8360.
[5] T. B. Geijtenbeek, R. Torensma, S. J. van Vliet, G. C. F. van Duijnhoven, G. J. Adema, Y. van Kooyk, C. G. Figdor, *Cell* **2000**, *100*, 575 – 585.
[6] T. B. Geijtenbeek, D. S. Kwon, R. Torensma, S. J. van Vliet, G. C. F. van Duijnhoven, J. Middel, I. L. M. H. A. Cornelissen, H. S. L. M. Nottet, V. N. KewalRamani, D. R. Littman, C. G. Figdor, Y. van Kooyk, *Cell* **2000**, *100*, 587 – 597.
[7] F. Halary, A. Amara, H. Lortat-Jacob, M. Messerle, T. Delaunay, C. Houles, F. Fieschi, F. Arenzana-Seisdedos, J. F. Moreau, J. Dechanet-Merville, *Immunity* **2002**, *17*, 653 – 664.
[8] C. P. Alvarez, F. Lasal, J. Carrillo, O. Muniz, A. L. Corbi, R. Delgado, *J. Virol.* **2002**, *76*, 6841 – 6844.
[9] B. Tassaneetrithep, T. H. Burgess, A. Granelli-Piperno, C. Trumpfheller, J. Finke, W. Sun, M. A. Eller, K. Pattanapanyasat, S. Sarasombath, D. L. Birx, R. M. Steinman, S. Schlesinger, M. A. Marovich, *J. Exp. Med.* **2003**, *197*, 823 – 829.
[10] P. Y. Lozach, H. Lortat-Jacob, A. De Lacroix de Lavalette, I. Staropoli, S. Foung, A. Amara, C. Houles, F. Fieschi, O. Schwartz, J. L. Virelizier, F. Arenzana-Seisdedos, R. Altmeyer, *J. Biol. Chem.* **2003**, *278*, 20358 – 20366.
[11] S. Pöhlmann, J. Zhang, F. Baribaud, Z. Chen, G. J. Leslie, G. Lin, A. Granelli-Piperno, R. W. Doms, C. M. Rice, J. A. McKeating, *J. Virol.* **2003**, *77*, 4070 – 4080.
[12] M. Colmenares, A. Puig-Kroger, O. M. Pello, A. L. Corbi, L. Rivas, *J. Biol. Chem.* **2002**, *277*, 36766 – 36769.
[13] A. Cambi, K. Gijzen, I. J. M. de Vries, R. Torensma, B. Joosten, G. J. Adema, M. G. Netea, B. J. Kullberg, L. Romani, C. G. Figdor, *Eur. J. Immunol.* **2003**, *33*, 532 – 538.
[14] T. B. Geijtenbeek, S. J. van Vliet, E. A. Koppel, M. Sanchez-Hernandez, C. M. Vandenbroucke-Grauls, B. Appelmelk, Y. van Kooyk, *J. Exp. Med.* **2003**, *197*, 7 – 17.
[15] N. Maeda, J. Nigou, J. L. Herrmann, M. Jackson, A. Amara, P. H. Lagrange, G. Puzo, B. Gicquel, O. Neyrolles, *J. Biol. Chem.* **2003**, *278*, 5513 – 5516.
[16] E. J. Tailleux, R. Barten, J. Trowsdale, *J. Immunol.* **2000**, *165*, 2937 – 2942.
[17] I. van Die, S. J. van Vliet, A. K. Nyame, R. D. Cummings, C. M. Bank, B. Appelmelk, T. B. Geijtenbeek, Y. van Kooyk, *Glycobiology* **2003**, *13*, 471 – 478.
[18] H. Feinberg, D. A. Mitchell, K. Drickamer, W. I. Weis, *Science* **2001**, *294*, 2163 – 2166.
[19] Y. Guo, H. Fienberg, E. Conroy, D. A. Mitchel, R. Alvarez, O. Blixt, M. E. Taylor, W. I. Weis, K. Drickamer, *Nat. Struc. Mol. Biol.* **2004**, *11*, 591 – 598.
[20] D. A. Mitchell, A. J. Fadden, K. Drickamer, *J. Biol. Chem.* **2001**, *276*, 28939 – 28945.
[21] A. Cambi, F. de Lange, N. M. van Maarseveen, M. Nijhuis, B. Joosten, E. M. H. P. van Dijk, B. I. de Bakker, J. A. M. Fransen, P. H. M. Bovee-Geurts, F. N. van Leeuwen, N. F. van Hulst, C. G. Figdor, *J. Cell Biol.* **2004**, *164*, 145 – 155.
[22] Y. Sako, T. Yanagida, *Nat. Cell Biol.* **2003**. Suppl. S, SS1 – SS5.
[23] D. J. Stephens, V. J. Allan, *Science* **2003**, *300*, 82 – 86.
[24] E. Betzig, J. K. Trautman, *Science* **1992**, *257*, 189 – 195.
[25] K. I. Willig, S. O. Rizzoli, V. Westphal, R. Jahn, S. W. Hell, *Nature* **2006**, *440*, 935 – 939.
[26] M. Gustafsson, *Proc. Natl. Acad. Sci. USA* **2005**, *102*, 13081 – 13086.
[27] E. Betzig, G. H. Patterson, R. Sougrat, O. W. Lindwasser, S. Olenych, J. S. Bonifacino, M. W. Davidson, J. Lippincott-Schwartz, H. F. Hess, *Science* **2006**, *313*, 1642 – 1645.
[28] F. de Lange, A. Cambi, R. Huijbens, B. I. de Bakker, W. Rensen, M. F. Garcia-Parajo, N. F. van Hulst, C. G. Figdor, *J. Cell Sci.* **2001**, *114*, 4153 – 4160.
[29] A. Ianoul, D. Grant, Y. Rouleau, M. Bani-Yaghoub, L. Johnston, J. P. Pezacki, *Nat. Chem. Biol.* **2005**, *1*, 196 – 202.
[30] M. Koopman, A. Cambi, B. I. de Bakker, B. Josten, C. G. Figdor, N. F. van Hulst, M. F. Garcia-Parajo, *FEBS Lett.* **2004**, *573*, 6 – 10.
[31] M. P. Gordon, T. Ha, P. R. Selvin, *Proc. Nat. Acad. Sci. USA* **2004**, *101*, 6462 – 6465.
[32] M. Vrljic, S. Y. Nishimura, S. Brasselet, W. E. Moerner, H. M. McConnell, *Biophys. J.* **2002**, *83*, 2681 – 2692.
[33] P. Keller, D. Toomre, E. Diaz, J. White, K. Simons, *Nat. Cell Biol.* **2001**, *3*, 140 – 149.
[34] S. Mañez, G. del Real, C. Martinez, *Nat. Rev. Immunol.* **2003**, *3*, 557 – 568.

Received: March 6, 2007
Revised: May 3, 2007
Published online on June 19, 2007

